analytical chemistry

pubs.acs.org/ac Article

UCL-MetIsoLib: A Public High-Resolution Tandem Mass Spectrometry Library for HILIC-Based Isomer-Resolved Profiling of Glycolysis, Central Carbon Metabolism, and Beyond in Urine, Plasma, Tissues, Cells, and Patient-Derived Organoids

Kristian Serafimov,* Maria Virginia Giolito, Sébastien Ibanez, Ophélie Renoult, Sarah Srhir, Paula Varon Rugeles, Florine Laloux-Morris, Cyril Corbet, Julien Pierrard, Marc Van den Eynde, Michael Lämmerhofer, and Olivier Feron

Cite This: *Anal. Chem.* 2025, 97, 21466−21474 Read Online

ACCESS | Metrics & More | Article Recommendations | Supporting Information

ABSTRACT: We present UCL-MetIsoLib, a publicly accessible high-resolution tandem mass spectrometry (HRMS/MS) library developed for HILIC-based, ion-pairing-free, isomer-resolved metabolomics using a bioinert UHPLC system and the Acquity Premier BEH Amide column. The platform integrates two complementary methods operating under distinct chromatographic conditions (pH 3.5, ESI^+; pH 11.0, ESI^-), enabling broad metabolic coverage. A total of 334 metabolites are annotated in the library structure, with thiol derivatization incorporated into the extraction protocol to mitigate redox-driven artifacts. Metabolite identification is supported by 245 authentic reference standards and curated according to MSI Level 1 and Level 2 criteria. Validation followed FDA guidelines for bioanalytical method validation across five biological matrices—urine, plasma, tissues, cells, and patient-derived colorectal organoids. The method demonstrated high precision (<15% RSD intra/inter-day) and recovery (85−115% across all QC levels). To demonstrate biological applicability, UCL-MetIsoLib was applied to a case study comparing healthy and colorectal cancer-derived organoids. The method enabled confident annotation of metabolite isomers, including key glycolytic intermediates such as DHAP and GA3P, as well as sugar phosphates from the glycolysis and pentose phosphate pathways. Metabolic alterations were observed in tumor organoids, including accumulation of nucleotide derivatives and shifts in central carbon metabolism. The library is constantly under expansion and is freely available in its latest version at: https://github.com/kserafimov10/UCLMetIsoLib.

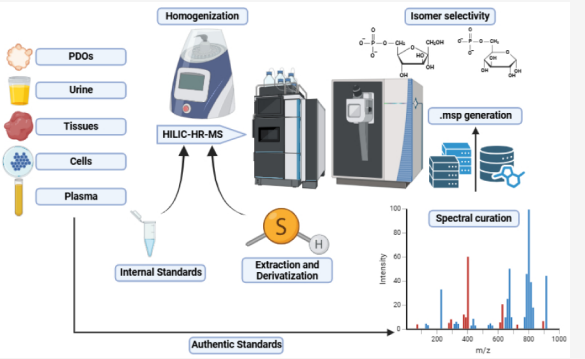

INTRODUCTION

High-resolution mass spectrometry (HRMS) has become a cornerstone of untargeted metabolomics, enabling the detection of thousands of features in complex biological matrices.[1,2] However, the confident identification of these metabolites remains a major bottleneck, particularly for structurally related compounds and isomers that cannot be distinguished based on m/z values alone.[3,7,8] The annotation challenge is further compounded by the diversity of sample types encountered in translational research—including biofluids, tissues, cell cultures, and emerging patient-derived models such as organoids—each introducing unique matrix effects and analytical variability.[3,9] While public MS/MS spectral libraries such as HMDB, MassBank, and GNPS have accelerated metabolite annotation efforts,[4−6] they often lack critical contextual information such as chromatographic retention times, ionization mode specificity, and validation across biological matrices.[6,7] Moreover, these resources typically do not resolve isomeric compounds, many of which share near-identical fragmentation patterns, leading to ambiguous or incorrect annotations in data-dependent acquisition (DDA) workflows.[2,8] There is a pressing need for high-quality, matrix-aware MS/MS reference libraries that enable isomer-resolved metabolite identification using reproducible and accessible analytical platforms.[3,7,9] In this context, hydrophilic interaction liquid chromatography (HILIC) has emerged as the preferred separation technique for polar and semipolar metabolites. HILIC is favored in metabolomics for its ability to retain polar analytes without ion-pairing reagents and its strong compatibility with ESI-MS.[10−16] Various

Received: June 6, 2025
Revised: August 5, 2025
Accepted: September 15, 2025
Published: September 22, 2025

https://doi.org/10.1021/acs.analchem.5c03390
Anal. Chem. 2025, 97, 21466−21474

stationary phases have been described in the literature, with zwitterionic sulfobetaine-coated[17−20] and amide-linked[21−23] phases being the most used in metabolomics studies. Undoubtedly, HILIC presents certain analytical challenges, specifically the frequently encountered issue of shifting retention times, for which a solution has recently been proposed.[24] However, the most significant challenge in HILIC metabolomics studies remains the accurate separation of molecular isomers and potential metabolites that may interconvert in the ion source during ionization process as a result of in-source fragmentation e.g., fumarate/malate, AMP/ADP/ATP (attributable to other nucleotides as well). There are numerous isomeric species among multiple biochemical pathways that are of critical importance in every biological sample e.g., sugar phosphates and their metabolites related to the glycolysis and pentose phosphate pathway,[25−27] nitrous oxide cascade related metabolites such as asymmetric and symmetric dimethylarginine (ADMA/SDMA),[28] sugars,[29] organic acids[30,31] and many more. Further complicating untargeted metabolomics workflows are additional isomeric or structurally related metabolite pairs. Citrate and isocitrate, key intermediates of the TCA cycle, are difficult to resolve chromatographically due to their nearly identical structures. Amino acid isomers such as leucine and isoleucine exhibit near-identical MS/MS fragmentation patterns, complicating confident annotation. Methylmalonate and succinate represent another pair of structurally related metabolites relevant to mitochondrial and vitamin B12 metabolism, which are challenging to separate under standard HILIC conditions. Other notable examples include choline and betaine, compounds central to methyl group metabolism and osmoregulation, and nucleotide sugars like UDP-glucose and UDP-galactose, which are critical in glycosylation pathways yet difficult to resolve without tailored chromatographic strategies. Even redox cofactors such as NAD^+, NADH, $NADP^+$, and NADPH can exhibit overlap due to similar retention characteristics and fragment spectra. In many of these cases, tandem mass spectrometry alone does not suffice to solve the issue of assay specificity, as the obtained product ions are not characteristic of the individual metabolite, with the only differences being in the MS^2-fragment ratios.[32] Additionally, the choice of chromatographic hardware plays a crucial role in metabolomics analysis. Conventional liquid chromatography systems often incorporate stainless steel components, which can present challenges when analyzing polar and labile metabolites. Stainless steel surfaces are prone to adsorbing certain analytes, especially phosphate- and carboxylate-containing metabolites, leading to reduced recovery, peak tailing, and overall signal suppression. These interactions can compromise data reproducibility and metabolite coverage, particularly for metabolomics workflows aimed at capturing a broad range of small, polar compounds. To mitigate these issues, the implementation of biocompatible LC systems—utilizing inert materials such as PEEK (polyether ether ketone) and various alloys for fluidic pathways (e.g., MP35N, as used in this study)—has gained attention. These systems minimize nonspecific analyte adsorption and metal-induced degradation, ensuring improved metabolite recovery and enhanced chromatographic performance. Considering all of the above, we introduce UCL-MetIsoLib, a publicly available HRMS/MS library developed at the IREC Metabolomics Facility, specifically designed for HILIC-based isomer-resolved metabolomics.[33]

The library comprises 334 curated metabolites, acquired under optimized dual-polarity conditions, and includes both MSI Level 1 and Level 2 annotations supported by 245 authentic standards and in silico spectral verification. The method was analytically validated across five biological matrices—urine, plasma, tissues, cultured cells, and patient-derived organoids—in accordance with FDA bioanalytical guidelines, making it directly applicable to both experimental and clinical metabolomics workflows. The methodology described herein includes rapid, simultaneous extraction and derivatization of thiol-containing metabolites using *N*-ethylmaleimide (NEM). This step is essential because thiols are highly reactive and prone to oxidation and interconversion during sample handling and electrospray ionization (ESI), as the ion source represents a redox-active environment. Derivatization stabilizes these redox-sensitive compounds, preserving their in vivo state and enabling accurate quantification. Given the critical role of thiols in cellular redox regulation, their reliable detection is key to understanding redox dynamics in biological systems. To demonstrate its utility, we applied UCL-MetIsoLib to a case study comparing healthy and metastatic colorectal cancer organoids. All curated MS/MS spectra are provided as .txt files in the Supporting Information, making UCL-MetIsoLib a ready-to-use, open-access resource for the metabolomics community (Figure 1).

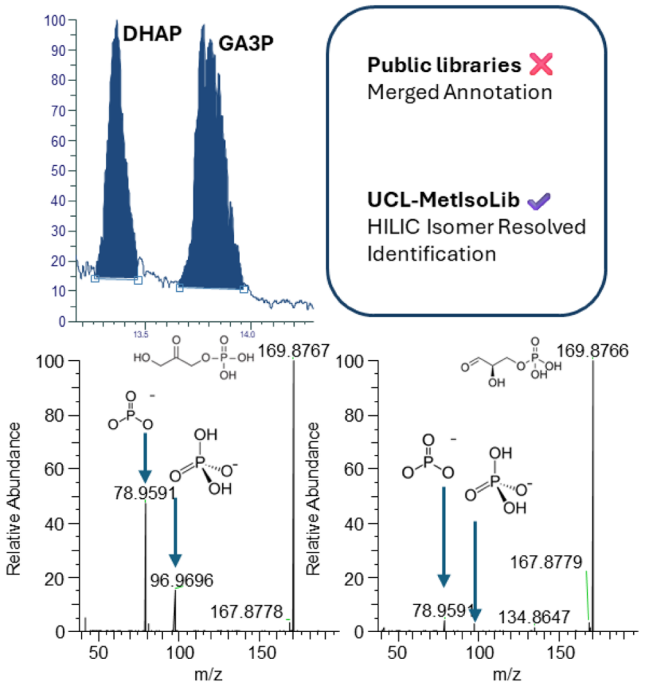

Figure 1. Isomer-resolved annotation of DHAP and GA3P using UCL-MetIsoLib. HILIC-based chromatographic separation of the isomeric sugar phosphates dihydroxyacetone phosphate (DHAP) and glyceraldehyde 3-phosphate (GA3P) demonstrates baseline resolution using the validated dual-polarity method. Despite nearly identical MS/MS fragmentation patterns in negative mode—both producing diagnostic phosphate-related ions at *m/z* 78.9591 (PO_3^-) and 96.9696 ($H_2PO_4^-$)—UCL-MetIsoLib enables confident differentiation based on retention time.

https://doi.org/10.1021/acs.analchem.5c03390
Anal. Chem. 2025, 97, 21466−21474

EXPERIMENTAL SECTION

Materials. Formic acid, acetic acid and acetonitrile of Ultra LC−MS grade were supplied by Fisher Scientific (Brussels, Belgium). Ammonium hydroxide solution (Suprapur quality 25% NH_3 basis), NIST Plasma and *N*-ethylmaleimide was purchased from Sigma-Aldrich (Merck, Hoeilaart, Netherlands). Uniformly U−^{13}C, U−^{15}N-labeled Amino Acid Mixture was obtained from Buchem BV (Apeldoorn, Netherlands). All standards used in this study were provided by Sigma-Aldrich (Merck, Hoeilaart, Netherlands). PFA bottles for mobile phases were provided by AHF Analysentechnik (Tübingen, Germany).

Organoid Culture. The colorectal cancer (CRC) organoid model was generated from colon cancer tissue obtained from a patient undergoing surgery at Cliniques Universitaires St. Luc in Brussels (ethics committee approval ONCO-2015-02 updated on 13-05-2019 following the principles of the Declaration of Helsinki). The CRC-N organoid model was derived from an adjacent healthy colon of a patient undergoing surgery (ethics committee approvals B4032020000038 and B4032023000027) in accordance with the Declaration of Helsinki. Signed informed consent was obtained, and personal data remained confidential. All CRC organoid cultures were plated in 50-μL domes of Cultrex Basement Membrane Extract, Type 2 (#3532-010-02, Bio-Techne) and maintained in Advanced DMEM/F12 (Thermo Fisher Scientific) supplemented with 1% Glutamax (Thermo Fisher Scientific), 1% HEPES (Thermo Fisher Scientific), 1% penicillin-streptomycin (Thermo Fisher Scientific), 1% B27 without vitamin A (Thermo Fisher Scientific), 1% N2 supplement (Thermo Fisher Scientific), 50 ng/mL EGF (STEMCELL Technologies), 10 mM nicotinamide (Sigma-Aldrich), and 1.25 mM *N*-acetyl cysteine (Sigma-Aldrich). CRC-N medium was further supplemented with 10 nM gastrin (Sigma), 0.5 nM hWNT3 surrogate (Thermo Fisher), 250 ng/mL R spondin-1, 100 ng/mL Noggin, 500 nM A-8301, and 10 μM SB202190 (STEMCELL Technologies). Organoids were typically passaged every 7−10 days, and the medium was changed every 2−3 days. Eight wells of 50 μL were pooled for metabolomic studies. Organoids were recovered using 500 μL Gentle Cell Dissociation Reagent (STEMCELL Technologies). The dome was scraped with a P1000, incubated on ice, then centrifuged for 5 min (400 g, 4 °C). The pellet was washed three times with cold PBS and constantly kept on ice. The organoids were transferred to a preweighted 1.5-mL tube, centrifuged, and then snap-frozen in liquid nitrogen. After freezing, the tubes containing the organoid pellets were weighed to calculate the organoid mass for normalization. Pellets were stored at −80 °C.

Cell Culture. The human CRC cell line (HCT-116) was purchased from ATCC (Manassas, Virginia, USA). The cells were cultured in DMEM (61965.026, Gibco) supplemented with 10% heat-inactivated FBS (F7524, Merck) and 1% penicillin/streptomycin (15140-122, Gibco). After reaching 80% confluence, cells were washed with cold PBS, frozen by liquid nitrogen contact and scraped.

Animal Experiments. Rj:NMRI-Foxn1nu/nu 5-week-old female mice were purchased from Janvier and housed in room with 12 h light/12 h dark cycles. Experimental procedure was authorized by the local ethical committee (reference 2020−032). After accommodation, mice were injected subcutaneously with 2 × 10^6 FaDu cells in 0.9% NaCl. Mice were weighed once per week and tumors were measured 3 times a week. Mice were sacrificed when tumors reached 600 mm^3, and tumors were collected and immediately snap-frozen in liquid nitrogen.

Sample Preparation and Metabolite Extraction. Cell, tissue and organoid samples were prepared in homogenization tubes. One mL of extraction solvent was added (50/50 *v*/*v* MeOH/H_2O with the MeOH fraction containing 20 mM of N-Ethylmaleimide (NEM) for derivatization), 20 μL internal standard solution of U−^{13}C, U−^{15}N-labeled amino acid mixture and 0.15 g 1.0 mm zirconia/glass beads for homogenization of cells and organoids, for tissues, the same amount of zirconia/glass beads was used but in a diameter of 1.4 mm. Derivatization and extraction have been performed as previously described.[12,34] In brief, post addition of the extraction solvent samples were left to react at room temperature for 15 min. Quenching of the reaction followed with the addition of 10 μL concentrated formic acid. Thereafter the samples were homogenized at 4 °C for 10 cycles (10 s per cycle, 5000 rpm, pause 30 s for cells and organoids and 30 s per cycle, 8000 rpm, pause 30 s for tissues) with Precellys Evolution high performance cell lyser (Bertin Technologies, France). The samples were then spun down for 10 min (20000 *g* at 4 °C), the supernatant removed and spun down once more for 10 min (20000 *g* at 4 °C). The supernatant was then removed and evaporated to dryness with a high-performance evaporator (Genevac EZ-2) (Genevac, Ipswich, UK). Reconstitution was performed in 50 μL ACN/H_2O (50/50; v/v). After reconstitution, the sample was vortexed for 10 s and spun down for 10 min (20,000 *g*, 4 °C). The supernatant was taken and placed on a Whatman Puradisc 4 syringe filter (PTFE, 0.2 μm) fixed inside a 1.5 mL Eppendorf tube. By centrifuging for 2 min at 10,000 *g* at 4 °C, sample filtration was performed for extra purification and the filtered sample transferred to UHPLC vials equipped with silanized microinserts for sample analysis. In the case of urine and plasma, the steps were identical with no homogenization required. Sample amounts this protocol is based on are 100 μL of plasma, 500 μL of urine, 50 mg of tumor tissue, 3 million cells and 50 mg of patient derived colorectal organoid matrix.

Untargeted HILIC-HR-MS Analysis. LC−MS analysis was performed on a Thermo Fisher (Dilbeek, Belgium) Vanquish Horizon system equipped with a binary pump, autosampler and thermostated column compartment. Chromatographic separation was performed on a Waters (Antwerp, Belgium) Acquity Premier VanGuard-FIT BEH Amide column (100 × 2.1 mm, 1.7 μm), equipped with a VanGuard-FIT BEH Amide precolumn (5 × 2.1 mm, 1.7 μm). Silanized microinserts were used during sample analysis to limit the interaction between phosphorylated compounds and glass surfaces. For metabolite analysis in ESI$^+$ mode, a stock solution of 500 mM LC−MS grade formic acid was prepared and adjusted to a pH of 3.5 with ammonium hydroxide. A following 1:10 dilution with water (mobile phase A) and with acetonitrile (mobile phase B) resulted in the final mobile phase conditions used during sample analysis in positive ionization mode. The chromatographic gradient was as follows: (0.0 min, 100% B; 20 min 70% B; 21 min 70% B; 21.01 min 100% B; 30 min 100% B) and a flow rate of 0.2 mL min^{-1} was used. The chromatographic separation in ESI$^-$ mode differed. An aqueous stock solution of 1000 mM ammonium hydroxide was prepared and adjusted to a pH of 11.0 with formic acid. After a subsequent dilution of 1:10 with water (mobile phase A) and with acetonitrile

https://doi.org/10.1021/acs.analchem.5c03390
Anal. Chem. 2025, 97, 21466−21474

(mobile phase B) the desired mobile phase conditions were achieved. Gradient elution followed a 2-step pattern and was performed as follows: (0.0 min, 95% B; 20 min 85% B; 25 min 60% B; 25.01 min 95% B; 30 min 95% B) and was carried out at a flow rate of 0.5 mL min^{-1}. During both methods, a constant column temperature of 60 °C was maintained throughout the entire analytical run and in both cases the injection volume was 3 μL. The autosampler was kept at 4 °C. Mobile phases were kept stirred and at 50 °C throughout the analysis. Ion source parameters were as follows: In negative mode: sheathe gas (50, nitrogen), aux gas (10, nitrogen), sweep gas (0 psi, nitrogen), ion transfer tube temperature (325 °C), ion source voltage −3000 V (negative mode), vaporizer temperature (350 °C). In positive mode—sheathe gas (35, nitrogen), aux gas (7, nitrogen), sweep gas (0 psi, nitrogen), ion transfer tube temperature (325 °C), ion source voltage +3500 V (negative mode), vaporizer temperature (275 °C). Analytes were recorded via a full scan with a mass resolving power of 11250 over a mass range from 70 to 900 m/z (scan time: 100 ms, RF lens: 70%). Normalized AGC Target was set to 500% (ESI^+) and 500% (ESI^-), Maximum Injection Time 150 ms and 1 Microscans were additional settings. To obtain MS/MS fragment spectra, data-dependent acquisition was carried out at a resolving power of 11250 over a mass range from 70 to 900 m/z and an isolation window of 2 m/z. RF lens was set to 70%, TopN was adjusted 10, Microscans set to 1, AGC Target was set to 50% (ESI^+) and 50% (ESI^-) with a Maximum Injection Time of 50 ms. Collision Energy was Nomalized to 30/50/70%. Dynamic Exclusion, Targeted Mass and Apex Detection were utilized as scan filters. Dynamic Exclusion Mode was operated in the custom setting (exlude after 1 hits for 10 s), Targeted Mass involved the utilization of an in-house metabolite inclusion list and Apex Detection was set to 30%. Blank solvents (mobile phase A and B) were injected in the beginning of the chromatographic batch to ensure proper column and system equilibration. Samples were first analyzed in negative and subsequently in positive ionization mode in randomized order. Data processing comprising peak finding, blank subtraction, feature alignment, normalization, MS/MS spectral deconvolution and score-based metabolite identification was performed with MS-DIAL software (version 4.9.221218).[34] A similarity score of 80% was chosen as threshold for reliable metabolite identification. All metabolite annotations were supported by retention time matching, precursor mass, and MS^2 spectral similarity against authentic standards and a curated in-house spectral library. Identification levels were assigned following the MSI guidelines (Level 1 corresponding to confirmed identity by authentic reference standard and Level 2 based on spectral MS/MS identification). An annotated metabolite list from the PDO metabolomics analysis with Log2 Fold Change, p-Values, Retention Times, MS/MS Fragments, and Precursor m/z is provided as part of the manuscript in the Supporting Information under Table S1. Normalization of metabolite intensities was performed using two complementary approaches: (1) Consideration of the biological variance of the material i.e., normalization to the wet weight of the organoid pellet, weight of the specific tissue, cell number or creatinine concentration in the case of urine (determined via LC−MS standard addition) to account for differences in biological input material, and (2) retention time proximity feature-specific normalization (B-MIS) using a U−^{13}C, U−^{15}N-labeled Amino Acid Mixture as internal standard. While this approach does not fully correct for ionization efficiency differences, it effectively reduces technical variability and offers a reproducible means of signal correction while at the same time serving as a practical compromise in complex biological matrices when class-specific standards are unavailable. Metabolites detected in less than 20% of samples were filtered out. Missing values for the remaining metabolites were imputed using Random Forest in Python. Metabolites with an p-value <0.05 and a fold-change greater than ±1.0 were considered significantly regulated. For peak finding an intensity threshold of 500 counts per second (cps) was selected. All further statistical processing and visualization were conducted with Python.

Method Validation. To assess method performance, PRM acquisiton was performed for a total of 245 authentic chemical standards with the previously mentioned ion source and chromatographic parameters. Determination of matrix effect (ME), extraction recovery (ER), and process efficiency (PE) followed the Matuszewski protocol.[35] ME was evaluated at a concentration level of 100 ng mL^{-1} in a pre- and postextraction spiking experiment with organoid cell matrix after as follows:

$$\mathrm{ME}\% = \frac{A_{\mathrm{spiked}} - A_0}{A_{\mathrm{neat}}} \quad (1)$$

With A_{spiked} being the area of the postextraction spiked organoid extract samples, A_0 the peak area of the analyte endogenously present in the cell extract (previously determined by LC−MS standard addition quantification) and A_{neat} the peak area of the selected metabolite in neat solution. In the same manner, ER and PE were evaluated at the same concentration level via pre- and postextraction spiked organoid extract samples and pre-extraction spiked versus neat standard solution, respectively. Calibration functions were generated by plotting normalized peak areas (peak area nominal divided by the peak area of the closest eluting isotope-labeled internal standard) versus the concentration of standard solutions (1, 50, 100, 500, and 1000 ng mL^{-1}). Matrix matched calibration was performed as well by spiking a series of 5 concentration levels (1, 50, 100, 500, and 1000 ng mL^{-1}) to the biological matrix (organoid matrix). Weighted linear regression ($1/x^2$) was used for both external and matrix-matched calibration curves. Linearity was evaluated by the determination of the regression coefficients (r^2) of the matrix matched calibration functions for each metabolite and by evaluating the back-calculation values of the concentrations of the nonzero calibrators regarding their nominal concentrations (spiked concentrations; endogenous amount as predetermined via LC-MS and standard addition corrected), which should be in at least 75% of calibrator levels ±15%. Further evaluation and validation of the developed method, including intra- and inter-run accuracy and precision was carried out in organoid extract samples according to the FDA guidelines for bioanalytical method validation at 4 different concentration levels (QC_{LLOQ}/QC_{low}/QC_{mid}/QC_{high} 10 ng mL^{-1}/50 ng mL^{-1}/500 ng mL^{-1}/1000 ng mL^{-1}). For the determination of LoDs and LoQs, the external calibration function was used for the individual metabolites as follows:

$$\mathrm{LoD} = \frac{3.3 \times \sigma}{m} \quad (2)$$

With σ being the standard error of the calibration function's slope and m the slope value itself. Analogous to the LoQ determination, the following equation was used:

https://doi.org/10.1021/acs.analchem.5c03390
Anal. Chem. 2025, 97, 21466−21474

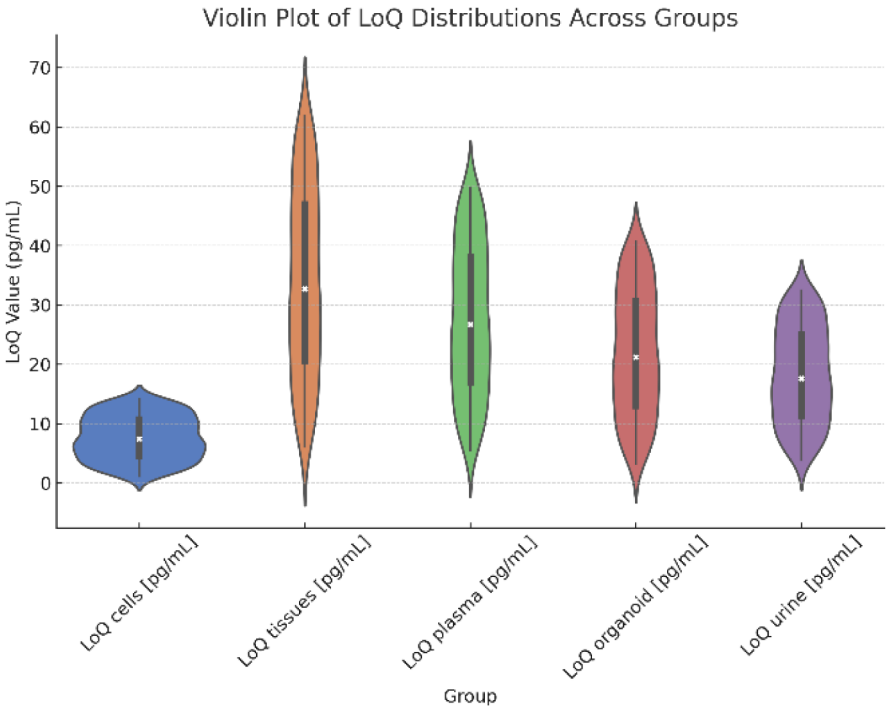

Figure 2. LoQ distribution comparison between 5 different types of biological matrix. Values in pg/mL.

$$\mathrm{LoQ} = \frac{10 \times \sigma}{m} \tag{3}$$

Individual metabolite accuracies (ACC) were calculated with quality control samples obtained by spiking organoid extract samples at four different concentration levels and corrected for endogenously present levels as

$$\mathrm{ACC\%} = \frac{c_{\mathrm{found}} - c_0}{c_{\mathrm{spiked}}} \tag{4}$$

With c_{spiked} being the concentration spiked to the organoid extract, c_0 the endogenously present amount (determined by LC−MS standard addition quantification) and c_{found} the concentration of the target metabolite found in the spiked sample.

Data Processing. Xcalibur was used for data acquisition and system control. Freestyle was used for data evaluation. Skyline was employed for peak integration and linear regression ($1/x^2$ as weight). Statistical analysis and visualization were performed with Python. MS-DIAL was used for metabolite curation and chromatographic batch alignment.

RESULTS AND DISCUSSION

Library Curation. The UCL-MetIsoLib library comprises 334 curated metabolites, distributed across two complementary acquisition modes using HILIC-based separation under distinct pH conditions: pH 3.5 for positive mode (ESI^+) and pH 11.0 for negative mode (ESI^-). All data were acquired on a high-resolution Orbitrap system using normalized collision energies (NCE) of 30, 50, and 70, capturing diverse and informative fragmentation profiles. Chromatographic separation was performed on a bioinert UHPLC system equipped with an Acquity Premier BEH Amide column, supporting high retention stability and resolution of polar and isomeric compounds. Spectra were curated from internally generated data sets, with manual inspection of all entries to ensure spectral quality, fragmentation logic, and chromatographic consistency. Annotation followed MSI Level 1 or Level 2 guidelines, supported by 245 authentic reference standards, while Level 2 annotations were cross validated through in silico fragmentation. Fragment curation and library export were supported by custom in-house Python scripts, which systematically filtered and consolidated spectral data. For each metabolite, multiple adduct forms were detected (e.g., $[M + H]^+$, $[M + Na]$, $[M + NH_4]^+$), and redundant spectra were collapsed to a single consensus entry. This was achieved by evaluating precursor mass proximity, retention time alignment, and shared high-intensity fragment ions across adduct types. Fragment selection was based on reproducibility across collision energies and ranked using a weighted scoring system favoring signal intensity, m/z coverage, and adduct relevance. This ensured that the final .txt files included only the most informative and nonredundant fragmentation patterns for each compound. Spectral similarity between experimental MS/MS and in silico predictions was assessed using a cosine similarity metric, calculated via vector normalization of m/z and intensity pairs:

$$\text{cosine score} = (\Sigma A_i \cdot B_i)/(\sqrt{\Sigma A_i^2} \cdot \sqrt{\Sigma B_i^2}) \tag{5}$$

where A_i and B_i represent the intensities of the ith matched fragment ion in the experimental and predicted spectra, respectively. Only matches exceeding a cosine score threshold of ≥ 0.7 were retained for Level 2 annotation. In-house Python scripts also evaluated dot product and reverse dot product scores to rank adduct-specific spectra, ensuring selection of the most representative fragmentation pattern per metabolite. Notable ionization trends were observed across compound classes: nucleotides, phosphorylated metabolites, and CoA derivatives consistently showed stronger signals in negative mode, while amines, amino acids, and small polyamines preferentially ionized in positive mode. Finalized .txt files for both ionization modes are provided in the Supporting

https://doi.org/10.1021/acs.analchem.5c03390
Anal. Chem. 2025, 97, 21466−21474

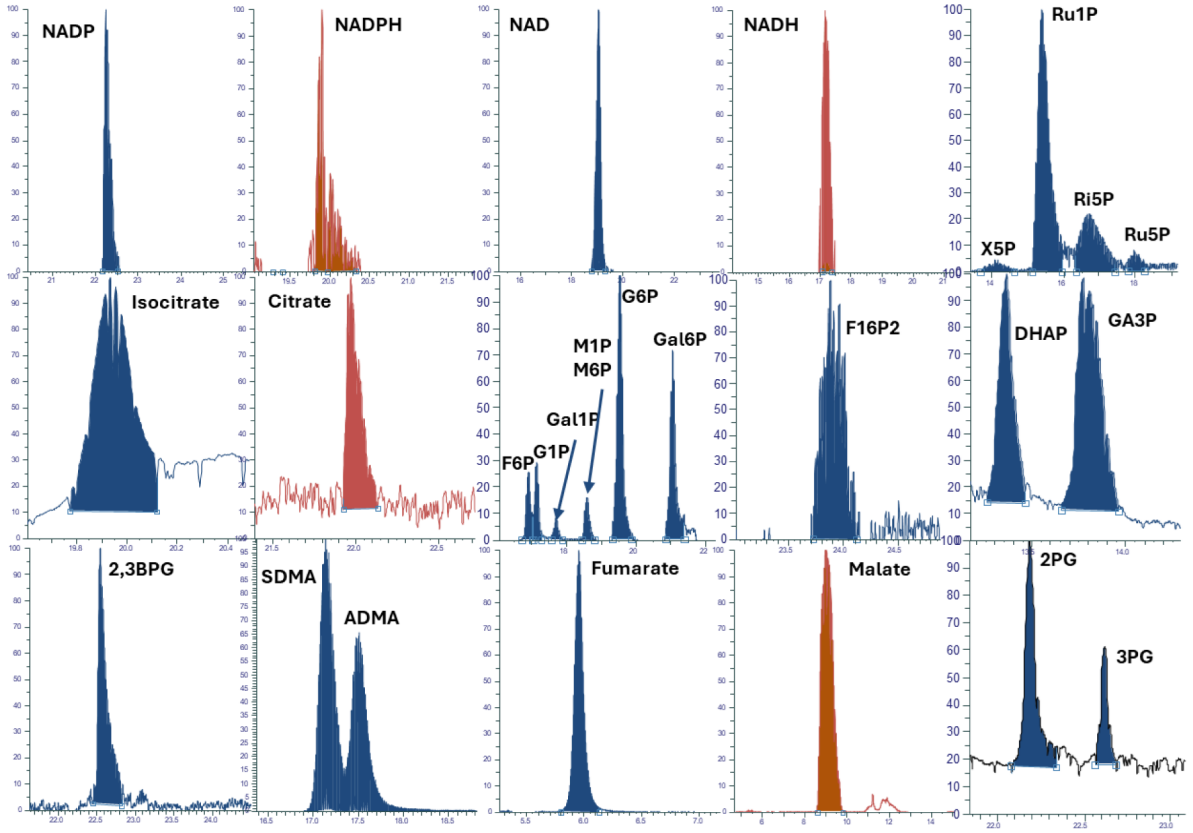

Figure 3. Chromatographic performance of chosen critical metabolites detected in human colorectal organoid samples.

Information and include curated metadata for each compound: precursor m/z, retention time, collision energy, polarity, HMDB ontology, SMILES, and InChI codes.

Method Performance. Method validation was conducted in accordance with FDA Bioanalytical Method Validation guidelines, assessing linearity, limits of detection and quantification (LoD/LoQ), precision, accuracy, recovery, process efficiency and matrix effects across five biological matrices: urine, plasma, tissues, cultured cells, and patient-derived colorectal organoids. A U−^{13}C, U−^{15}N-labeled Amino Acid Mixture was used as a universal internal standard across all matrices, ensuring matrix-matched normalization and controlling for extraction variability. Linearity was evaluated using 5-point calibration curves ranging from 500 pg/mL to 1 μg/mL, covering the expected physiological range of most endogenous metabolites. Quantification was based on MS^1 signal intensities, as MS^2 detection exhibited partial saturation at higher concentrations due to DDA acquisition limitations. According to FDA criteria, ≥ 85% of calibration points were required to fall within 85−115% of nominal values, which was achieved for all compounds across all matrices (Tables S7−S11). Limits of detection (LoD) and quantification (LoQ) were calculated using signal-to-noise ratios of 3 and 10, respectively. LoD and LoQ distributions demonstrated matrix-dependent trends, with the highest detection limits observed in tissue homogenates, followed by plasma, organoids, urine, and cells, which consistently produced the lowest background and highest sensitivity. These distributions are illustrated in Figure 2.

Matrix effects were assessed by comparing postextraction spiked standards to neat solutions and data is provided in Tables S2−S6. The most pronounced signal suppression was observed in tissues and plasma, particularly for nucleotides and polar phosphorylated compounds. Organoids and urine exhibited intermediate matrix effects, while cultured cells displayed minimal ion suppression, reflecting their lower matrix complexity. Precision, evaluated across intra- and interday replicate injections (n = 5 per QC level), remained below 15% relative standard deviation (RSD) for all compounds (Tables S12−S21). Inter- and intraday accuracy values across low, medium, and high concentrations ranged between 85−115%, meeting FDA bioanalytical criteria for all matrices and ionization modes (Tables S22−S31). In addition to baseline resolution of critical isomeric metabolite pairs such as citrate/isocitrate, fumarate/malate, isoleucine/leucine, and ADMA/SDMA, the optimized HILIC-MS workflow provided excellent separation of key sugar phosphates from central carbon metabolism. Specifically, hexose monophosphates, including glucose-1-phosphate (G1P), glucose-6-phosphate (G6P), fructose-6-phosphate (F6P), galactose-1-phosphate (Gal1P), and galactose-6-phosphate (Gal6P)—were successfully resolved (Figure 3). Despite their structural similarity and identical precursor ions, each metabolite eluted distinctly, enabling unbiased quantification across both glycolytic and galactose metabolism pathways. Furthermore, the pentose phosphate pathway intermediates ribose-5-phosphate (Ri5P), xylulose-5-phosphate (X5P), ribulose-1-phosphate (Ru1P), and ribulose-5-phosphate (Ru5P) were separated, supporting confident annotation of pentose phosphate pathway dynamics (Figure 3). Additional glycolytic intermediates, including glyceraldehyde-3-phosphate (GA3P) and dihydroxyacetone phosphate (DHAP), were also well resolved (Figure 3), eliminating ambiguity in the interpretation of lower glycolysis flux. Importantly, 2-phosphoglycerate (2-PG) and 3-phospho-

https://doi.org/10.1021/acs.analchem.5c03390
Anal. Chem. 2025, 97, 21466−21474

glycerate (3-PG) were baseline-separated (Figures 1, 3), overcoming one of the common chromatographic challenges in untargeted metabolomics. The successful separation of this cluster of sugar phosphate isomers underscores the method's robustness in handling polar and structurally similar metabolites from central carbon metabolism. These findings are particularly relevant for biological models such as tumor-derived organoids, where the precise resolution of glycolytic and pentose phosphate intermediates is crucial for the accurate interpretation of metabolic pathway fluxes. The sample preparation protocol incorporated thiol derivatization, which effectively stabilized redox-sensitive metabolites and minimized oxidative degradation during processing and analysis. Together, these results demonstrate the method's robustness, reproducibility, and broad applicability for quantitative metabolomics across a range of complex biological matrices.

Application. Post method validation, the current untargeted metabolomic workflow was applied to patient-derived colorectal organoids. Two groups of organoids were analyzed for further in-depth metabolic profiling—healthy and primary tumor organoids. Statistical analysis with the PCA (Figure S1) showed clear grouping of the individual samples. Volcano plots were generated, illustrating the two-sided comparison between healthy and primary tumor organoids (Figure 4).

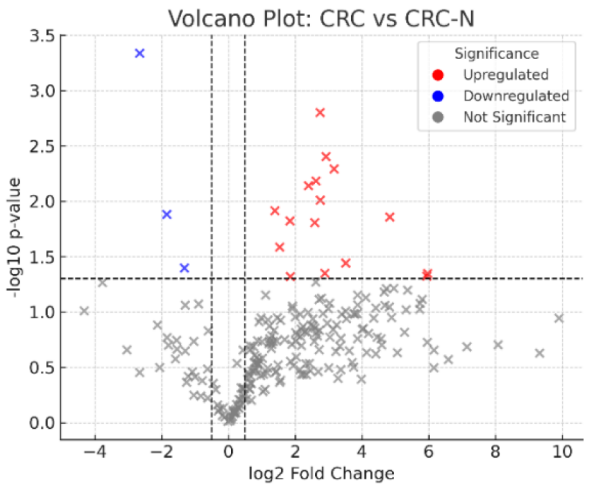

Figure 4. Volcano plot comparison between CRC organoid and CRC-N (healthy colorectal organoid). Significant up/downregulated metabolites marked in red/blue (p-value <0.05 and log2FC > ±1.0).

The resulting p-values and log2 fold changes from the two-sided T-Test analysis are provided in Table S1. Based on these results, boxplots of the significantly up- and downregulated metabolites were generated and presented in Figure S2, while Figure S3 provides an overview of the number of annotated metabolites in each biological matrix. Metabolomic profiling between colorectal cancer organoids (CRC) and healthy colon organoids (CRC-N) revealed significant remodeling of central carbon and nucleotide metabolism, consistent with tumor-specific metabolic reprogramming. Key TCA cycle and glycolytic intermediates were significantly elevated in CRC organoids. Citrate, a key metabolite in the TCA cycle, was upregulated, indicating enhanced mitochondrial activity. This suggests active oxidative metabolism, not only for ATP generation but also for supplying biosynthetic precursors (e.g., citrate export for fatty acid synthesis). 2-phosphoglycerate, a glycolytic intermediate upstream of phosphoenolpyruvate, was also increased, suggesting an augmented glycolytic flux. The presence of elevated 3-hydroxybutyrate reflects increased β-oxidation of fatty acids, potentially serving to fuel the TCA cycle or acting as a stress-adaptive energy source. Elevated levels of 2-hydroxyglutarate may reflect aberrant isocitrate dehydrogenase (IDH) activity, such as mutations in IDH1 or IDH2, or indicate broader mitochondrial metabolic dysregulation. Several nucleosides were significantly downregulated in CRC organoids. Adenosine and inosine levels were both suppressed, suggesting disruption in purine metabolism, particularly the nucleotide salvage pathway. These pathways are essential for maintaining nucleotide pools in rapidly dividing cells. However, tumor cells often rely on de novo nucleotide biosynthesis to meet the demands of high proliferation rates. The observed drop in salvage nucleosides may thus reflect a metabolic switch toward more energy-intensive biosynthetic routes, or alternatively, altered extracellular nucleotide turnover and purinergic signaling, both of which play roles in cell cycle progression, inflammation, and immune evasion. Additionally, creatinine, a byproduct of creatine metabolism involved in cellular energy buffering via the phosphocreatine system, was decreased, pointing to altered phosphagen dynamics. These findings highlight a CRC-specific metabolic signature supporting biosynthesis and proliferation.

CONCLUSION

We present UCL-MetIsoLib, a validated, high-resolution tandem mass spectrometry (HRMS/MS) library specifically designed for isomer-resolved metabolomics using dual-mode HILIC separation. The method employs a bioinert UHPLC system with an Acquity Premier BEH Amide column and has been analytically validated across five biologically relevant matrices—urine, plasma, tissues, cultured cells, and patient-derived organoids—in accordance with FDA bioanalytical guidelines. The library comprises 334 meticulously curated metabolites, with MSI Level 1 guaranteed by 245 authentic standards and Level 2 annotations, supported by in silico spectral verification. Notably, the method achieves robust isomer resolution through polarity-specific fragmentation and retention time filtering, features often lacking in public spectral repositories. To the best of our knowledge, this is the only methodological platform that combines this level of comprehensiveness and selectivity within a HILIC-based metabolomics framework.

ASSOCIATED CONTENT

Data Availability Statement

Latest version of the up-to-date held libraries can be found on: https://github.com/kserafimov10/UCLMetIsoLib.

Supporting Information

The Supporting Information is available free of charge at https://pubs.acs.org/doi/10.1021/acs.analchem.5c03390.

Information and data on chromatographic parameters such as ME, PE, ER; assay validation data values i.e., precision, accuracy, calibration; annotated peak list of metabolites in organoid study; fold change and statistical values for significant metabolites between both organoid models; figures related to the multivariate statistical analysis of both organoid models (PDF)

All curated MS/MS spectral data and associated metadata (TXT)

https://doi.org/10.1021/acs.analchem.5c03390
Anal. Chem. 2025, 97, 21466−21474

All curated MS/MS spectral data and associated metadata (TXT)

AUTHOR INFORMATION

Corresponding Author

Kristian Serafimov − *Institute de Recherche Expérimentale et Clinique (IREC), Pole of Pharmacology and Therapeutics, UCLouvain, Brussels 1200, Belgium; Institut de Recherche Expérimentale et Clinique (IREC) Metabolomics Core, UCLouvain, Brussels 1200, Belgium;* orcid.org/0009-0007-6982-6512; Email: kristian.serafimov@uclouvain.be

Authors

Maria Virginia Giolito − *Institute de Recherche Expérimentale et Clinique (IREC), Pole of Pharmacology and Therapeutics, UCLouvain, Brussels 1200, Belgium;* orcid.org/0000-0002-4888-7857

Sébastien Ibanez − *Institute de Recherche Expérimentale et Clinique (IREC), Pole of Pharmacology and Therapeutics, UCLouvain, Brussels 1200, Belgium*

Ophélie Renoult − *Institute de Recherche Expérimentale et Clinique (IREC), Pole of Pharmacology and Therapeutics, UCLouvain, Brussels 1200, Belgium*

Sarah Srhir − *Institute de Recherche Expérimentale et Clinique (IREC), Pole of Pharmacology and Therapeutics, UCLouvain, Brussels 1200, Belgium*

Paula Varon Rugeles − *Institute de Recherche Expérimentale et Clinique (IREC), Pole of Pharmacology and Therapeutics, UCLouvain, Brussels 1200, Belgium*

Florine Laloux-Morris − *Institute de Recherche Expérimentale et Clinique (IREC), Pole of Pharmacology and Therapeutics, UCLouvain, Brussels 1200, Belgium*

Cyril Corbet − *Institute de Recherche Expérimentale et Clinique (IREC), Pole of Pharmacology and Therapeutics, UCLouvain, Brussels 1200, Belgium*

Julien Pierrard − *Institut de Recherche Expérimentale et Clinique (IREC), Pole of Molecular Imaging, Radiotherapy and Oncology (MIRO), UCLouvain, Brussels 1200, Belgium; Radiation Oncology Department, Institut Roi Albert II, Cliniques Universitaires Saint-Luc, Brussels 1200, Belgium*

Marc Van den Eynde − *Institut de Recherche Expérimentale et Clinique (IREC), Pole of Molecular Imaging, Radiotherapy and Oncology (MIRO), UCLouvain, Brussels 1200, Belgium; Medical Oncology Department, Institut Roi Albert II, Cliniques Universitaires Saint-Luc, Brussels 1200, Belgium*

Michael Lämmerhofer − *Institute of Pharmaceutical Sciences, Pharmaceutical (Bio-)Analysis, University of Tübingen, Tübingen 72076, Germany;* orcid.org/0000-0002-1318-0974

Olivier Feron − *Institute de Recherche Expérimentale et Clinique (IREC), Pole of Pharmacology and Therapeutics, UCLouvain, Brussels 1200, Belgium; Institut de Recherche Expérimentale et Clinique (IREC) Metabolomics Core, UCLouvain, Brussels 1200, Belgium*

Complete contact information is available at: https://pubs.acs.org/10.1021/acs.analchem.5c03390

Notes

The authors declare no competing financial interest.

REFERENCES

(1) Patti, G. J.; Yanes, O.; Siuzdak, G. *Nat. Rev. Mol. Cell Biol* **2012**, *13* (4), 263−269.

(2) Misra, B. B.; van der Hooft, J. J. J. *Electrophoresis* **2016**, *37* (1), 86−110.

(3) Schrimpe-Rutledge, A. C.; Codreanu, S. G.; Sherrod, S. D.; McLean, J. A. *J. Am. Soc. Mass Spectrom* **2016**, *27* (12), 1897−1905.

(4) Wishart, D. S.; Guo, A.; Oler, E.; Wang, F.; Anjum, A.; Peters, H.; Dizon, R.; Sayeeda, Z.; Tian, S.; Lee, B. L.; et al. *Nucleic Acids Res* **2022**, *50* (D1), D622−D631.

(5) Horai, H.; Arita, M.; Kanaya, S.; Nihei, Y.; Ikeda, T.; Suwa, K.; Ojima, Y.; Tanaka, K.; Tanaka, S.; Aoshima, K.; et al. *J. Mass Spectrom* **2010**, *45* (7), 703−714.

(6) Wang, M.; Carver, J. J.; Phelan, V. V.; Sanchez, L. M.; Garg, N.; Peng, Y.; Nguyen, D. D.; Watrous, J.; Kapono, C. A.; Luzzatto-Knaan, T.; et al. *Nat. Biotechnol* **2016**, *34* (8), 828−837.

(7) Xiao, J. F.; Zhou, B.; Ressom, H. W. *TrAC, Trends Anal. Chem* **2012**, *32*, 1−14.

(8) Nicolardi, S.; Ursem, C.; Vos, D.; Kool, J.; Bovee, T. F. H.; van der Hooft, J. J. J. *Metabolites* **2022**, *12* (2), 132.

(9) Sumner, L. W.; Amberg, A.; Barrett, D.; Beale, M. H.; Beger, R.; Daykin, C. A.; Fan, T. W.-M.; Fiehn, O.; Goodacre, R.; Griffin, J. L.; et al. *Metabolomics* **2007**, *3* (3), 211−221.

(10) Hosseinkhani, F.; Huang, L.; Dubbelman, A.-C.; Guled, F.; Harms, A. C.; Hankemeier, T. *Metabolites* **2022**, *12* (2), 165.

(11) Virgiliou, C.; Sampsonidis, I.; Gika, H. G.; Raikos, N.; Theodoridis, G. A. *Electrophoresis* **2015**, *36* (18), 2215−2225.

(12) Serafimov, K.; Lämmerhofer, M. *J. Chromatogr. A* **2022**, *1684*, 463556.

(13) Spagou, K.; Tsoukali, H.; Raikos, N.; Gika, H.; Wilson, I. D.; Theodoridis, G. *J. Sep. Sci* **2010**, *33* (6−7), 716−727.

(14) Dekina, S.; Alexandrov, T.; Drotleff, B. *Metabolomics* **2024**, *20* (6), 114.

(15) Xing, S.; Yu, H.; Liu, M.; Jia, Q.; Sun, Z.; Fang, M.; Huan, T. *J. Am. Soc. Mass Spectrom* **2021**, *32* (9), 2296−2305.

(16) Gong, L.; McCullagh, J. S. O. *Rapid Commun. Mass Spectrom* **2014**, *28* (4), 339−350.

(17) Meister, I.; Zhang, P.; Sinha, A.; Sköld, C. M.; Wheelock, Å. M.; Izumi, T.; Chaleckis, R.; Wheelock, C. E. *Anal. Chem* **2021**, *93* (12), 5248−5258.

(18) Naz, S.; Gallart-Ayala, H.; Reinke, S. N.; Mathon, C.; Blankley, R.; Chaleckis, R.; Wheelock, C. E. *Anal. Chem* **2017**, *89* (15), 7933−7942.

(19) Lioupi, A.; Virgiliou, C.; Walter, T. H.; Smith, K. M.; Rainville, P.; Wilson, I. D.; Theodoridis, G.; Gika, H. G. *J. Chromatogr. A* **2022**, *1672*, 463013.

(20) Girel, S.; Guillarme, D.; Fekete, S.; Rudaz, S.; González-Ruiz, V. *J. Chromatogr. A* **2023**, *1697*, 463994.

(21) Kok, M. G. M.; Nix, C.; Nys, G.; Fillet, M. *Talanta* **2019**, *197*, 49−58.

(22) Sillner, N.; Walker, A.; Harrieder, E.-M.; Schmitt-Kopplin, P.; Witting, M. *J. Chromatogr. B* **2019**, *1109*, 142−148.

(23) Peterka, O.; Langová, A.; Jirásko, R.; Holčapek, M. *J. Chromatogr. A* **2025**, *1740*, 465588.

(24) Serafimov, K.; Knappe, C.; Li, F.; Sievers-Engler, A.; Lämmerhofer, M. *J. Chromatogr. A* **2024**, *1730*, 465060.

(25) Su, M.; Serafimov, K.; Li, P.; Knappe, C.; Lämmerhofer, M. *J. Chromatogr. A* **2023**, *1688*, 463727.

(26) Bajad, S. U.; Lu, W.; Kimball, E. H.; Yuan, J.; Peterson, C.; Rabinowitz, J. D. *J. Chromatogr. A* **2006**, *1125* (1), 76−88.

(27) Serafimov, K.; Lämmerhofer, M. *Anal. Chem* **2024**, *96* (43), 17271−17279.

(28) Bonnitcha, P.; Sullivan, D.; Fitzpatrick, M.; Ireland, A.; Nguyen, V. L.; Koay, Y. C.; O'Sullivan, J. *Pathology* **2022**, *54* (5), 591−598.

(29) Koley, S.; Chu, K. L.; Gill, S. S.; Allen, D. K. *J. Exp. Bot* **2022**, *73* (9), 2938−2952.

(30) King, A. M.; Mullin, L. G.; Wilson, I. D.; Coen, M.; Rainville, P. D.; Plumb, R. S.; Gethings, L. A.; Maker, G.; Trengove, R. *Metabolomics* **2019**, *15* (2), 17.

(31) Richardson, A. E.; Danielson, N. D. *Anal. Chim. Acta* **2017**, *996*, 98−105.

(32) Hsiao, J. J.; Potter, O. G.; Chu, T.-W.; Yin, H. *Anal. Chem* **2018**, *90* (15), 9457−9464.
(33) Serafimov, K.; Aydin, Y.; Lämmerhofer, M. *J. Sep. Sci* **2024**, *47* (1), No. e2300780.
(34) Tsugawa, H.; Cajka, T.; Kind, T.; Ma, Y.; Higgins, B.; Ikeda, K.; Kanazawa, M.; Van-DerGheynst, J.; Fiehn, O.; Arita, M. *Nat. Methods* **2015**, *12* (6), 523−526.
(35) Matuszewski, B. K.; Constanzer, M. L.; Chavez-Eng, C. M. *Anal. Chem* **2003**, *75* (13), 3019−3030.

https://doi.org/10.1021/acs.analchem.5c03390
Anal. Chem. 2025, 97, 21466−21474